Packaged bulk micromachined resonant force sensor for high temperature applications

M. Haueis[1], J. Dual, C. Cavalloni *, M. Gnielka*, R. Buser **
-
ETH Zürich, Institute of Mechanics, Tannenstrasse 3, CH-8092 Zürich, Switzerland
*Kistler Instrumente AG, CH-8408 Wintherthur, Switzerland
**NTB Buchs, CH-9471 Buchs, Switzerland

Abstract

We present a packaged microresonator for static load measurement under high temperatures, performing with high precision and a resolution better than 100 ppm. There is an industrial need a for such measurement tasks, however, such sensing cells are not available so far. To minimize temperature stress we developed an all-in-silicon solution, in difference to micromachined resonant force sensors, which have been published. We propose a force sensor where load coupling, the excitation and detection of the vibration of the microresonator are integrated in one and the same single crystal silicon package. The complete single crystal design together with a fiber-optical on-chip detection method will allow measurements at high temperatures. A considerable degree of freedom for the resonator's shape design, as needed for the investigation of filter mechanisms, is given by a DRIE fabrication method.

Keywords: Microresonator, Resonant sensor, load cell, Fabry-Perot Interferometer, MEMS, DRIE

1. Introduction

This paper describes design, fabrication and characterization of a force measuring unit with quasi digital output, which can be fabricated in batch processes such as used in microengineering's technology. The focus is a sensor part exhibiting a high sensitivity to applied stress with reliable performance in a high temperature environment. Bulk resonators and surface acoustic wave resonators are examples for resonating systems with quasidigital output [1]. Their response to varying boundary conditions is measurable through their change of resonant frequency and phaseshift. Much effort has been invested in the utilization of these features for stress, mass and temperature measurements as well as their use for filters in communication devices [2],[3],[4]. Strong industrial interests are focused on resonant sensors for load and pressure measurement [5], [6], [7]. Resonators based on single crystals such as silicon and quartz are of particular interest because single crystals combine high accuracy and repeatability and potentially low power consumption [8]. Materials like SiC, Diamond [9], Galliumorthophosphate have advantages for applications under high temperatures but have on the contrary the major drawback that they lack of advanced technology such as for silicon is available at this time.

2. Sensor design

The presented sensing cell consists of a SOI (silicon on insulator) handle wafer where the bending resonator, the excitation and the detection means are integrated and which is protected by a silicon lid. The design of our resonant structure is based on the required sensitivity (frequency shift versus force), the amplitude at resonance and the requirements of the readout electronics. For thermoelastic loss minimization the resonator was made to vibrate in a near isothermal mode. A linear electrostatic force is generated by an integrated comb shaped electrode, a principle which is compatible to high temperature

1. Corresponding author: ETH Zurich, Institute of Mechanical Systems, Tannenstrasse 3, CLA H21.2, tel: +41.1632.7792 fax: +41.1632.1145, e-mail: martin.haueis@imes.mavt.ethz.ch

applications. Two packaged chip designs were realized: one, where the vibration is detected capacitively (Type CAP: Figure 1), and one where the vibration is measured optically (Type OPT: Figure 2). For capacitive detection the problem of cross talk was solved by operating in closed loop with a switched lock-in amplifier [10], which resulted in a stable resonance behavior (Figure 10). Alternatively, for optical detection a Fabry-Perot-Interferometer is formed by a mirror-cut of a single mode fiber end face which is passively aligned to a high quality dry etched silicon side wall. In contrast to pressure sensors the crucial issue of the force sensor is the coupling of the force. We solved this by guiding the load from the metal housing via bolts to the silicon chip (Figure 12). On the silicon chip the force is translated from the bolts through a spring mechanism to the resonant structure. No gluing and a single material solution minimizes the temperature stress and makes the performance robust to high temperatures.

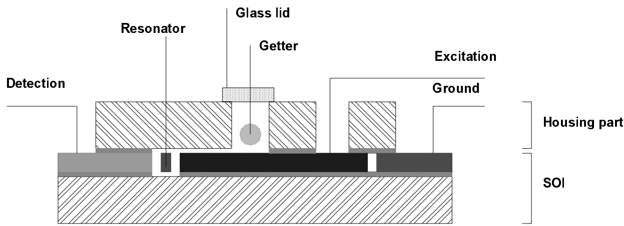

Figure 1 Schematic cross section perpendicular to the axis of a sensor with capacitive detection

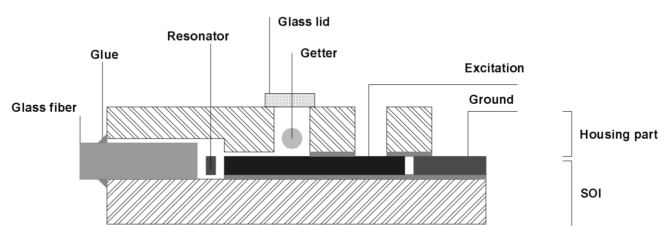

Figure 2 Schematic cross section perpendicular to the axis a of sensor with optical detection

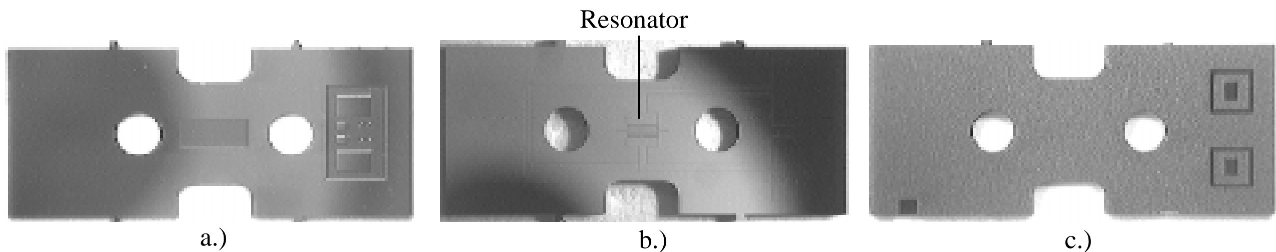

Figure 3 Fabricated resonant structures with capacitive detection: a.) inner side of housing part, b.) inner side of SOI with resonator in the center, c.) bonded package with electrodes and clamping holes

3. Resonant structure

The sensitivity to the measurand is a function of the resonator shape and the shunt force of the package. On the silicon chip the force is translated from the bolts through a spring mechanism to the resonant structure in order to match the maximum stress specifications of the resonant structure and to protect the cell against overload. The measurand force introduced to the sensing chip, in particular the frame, is split in a shunt force in the frame and a force loading the resonant structure itself. The stress experienced by the resonant structure is determined by the frame it is clamped on. The cell design presented has comparatively high shunt force so that the samples are safe for processing and for mounting into the metal housing. We optimized a resonant beam-mass system in the following way. First, we considered the boundary conditions for geometry set by technology, especially the aspect ratio of DRIE and the sensitivity to geometrical tolerances. Second, the resonator layout is determined by the desired Quality factor (Q-factor). A high Q-factor improves the frequency stability for a phase-locked oscillator loop, the amplitude and therefore the output signal of the detection circuit. Provided the resonator operates in a vacuum, where molecular damping is eliminated, the loss is governed by thermoelastic friction [11],[12]. Depending on the mode of operation, isothermal or adiabatic loss characteristics are distinguished. Two different beam dimensions satisfy the

required Q factor in these loss regimes. To match the frequency of available electronics and to be well under 100 kHz (calibration frequency for Quartz resonators) we designed a resonator operating in the isothermal mode at 25 kHz. We chose for the beam thickness 25 micrometer, while the height of the beam has to be in accordance to the technologically achievable aspect ratio (DRIE: about 18). For a 5 micrometer comb drive distance the etchable height becomes 80 micrometer. The mass dimensions and its perforation are chosen to match the required frequency, the load sensitivity and to allow space for the necessary number of combs. The number of combs is calculated from the desired deflection which is necessary for our capacitive sensing electronics (greater than 100 nm in resonance). The stable operation of a resonant sensor furthermore depends on its material properties which should exhibit a linear elastic behavior, no creeping, ideally no temperature dependence of its elastic properties and no internal stress. We selected Silicon as a single crystal material with a wide range of processing technologies available at this time.

Load sensitivity

The resonance frequency for a mass suspended by two beams (Figure 4) is governed by the general expression for a beam with stiffness, mass inertia, rotational inertia and shear effects (“Timoshenko beam”) [13]:

$$m' \cdot \frac{\partial^2}{\partial t^2} y[x,t] + E \cdot I \cdot \frac{\partial^4}{\partial x^4} y[x,t] - \frac{m' \cdot I}{A} \cdot \left(1 + \frac{E}{\kappa \cdot G}\right) \cdot \frac{\partial^2}{\partial t^2}\frac{\partial^2}{\partial x^2} y[x,t] = 0 \quad ,$$

where m' = mass per unit length, E = Youngs modulus, I = moment of bending inertia, A = area, G = shear modulus, $\kappa = 5/6$ for a rectancular cross section. Neglecting higher order terms and the contribution of shear forces and rotational inertia this equation is simplified to:

$$m' \cdot \frac{\partial^2}{\partial t^2} y[x,t] + E \cdot I \cdot \frac{\partial^4}{\partial x^4} y[x,t] = 0 \,.$$

The dependence of resonance frequency on applied load is approximated by the Rayleigh-Ritz Method which for a single beam was investigated in [5],[14] under consideration of different boundary conditions [15]. For the resonance frequency of a mass suspended by two beams vibrating in its first bending mode (Figure 5) we derived (see Appendix I):

$$\omega_o = \sqrt{127 \cdot \frac{E \cdot I}{l^3} \cdot \frac{1}{m'_A \cdot 0.254 \cdot l + 0.5 \cdot m \cdot C_y}} \,, \quad C_y = \frac{1}{1298} \,,$$

where l = length of the suspending beams, m = mass of the suspended mass. The application of a load F generates an axial stress in the suspending beams and shifts the resonance frequency of the first bending mode from ω_o to ω:

$$.\omega = \omega_o \left[1 + \frac{0.025 \cdot l^2 \cdot F}{E \cdot I}\right]^{\frac{1}{2}}$$

The sensitivity ratio between a beam having a suspended mass (denoted “A”) and a simple beam (denoted “B”), both assumed to have identical resonance frequencies, becomes:

$$r_S = \sqrt{\frac{m'_B}{m'_A}} \cdot \frac{1}{\sqrt{1 + \frac{250}{127} \cdot \frac{m}{m'_A} \cdot \frac{1}{l_A}}}$$

where m'_B = mass per unit length of single beam "B", m'_A = mass per unit length of suspending beams "A", l_A = length of both suspending beams "A". This expressions say, that for two beams with the same material properties, momentum of inertia for bending, cross section and resonance frequency, all these are parameters which are given by technology and electronics, the added mass decreases sensitivity as shorter the beams and as heavier the mass of the mesa become.

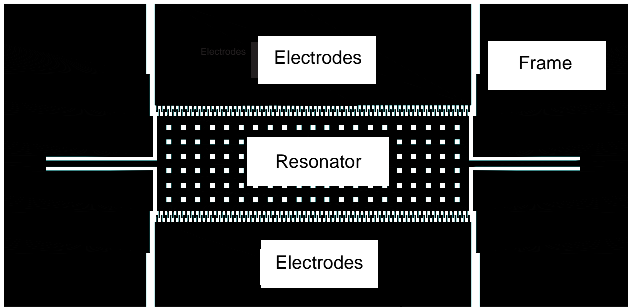

Figure 4 Resonant structure: perforated mass suspended on two beams

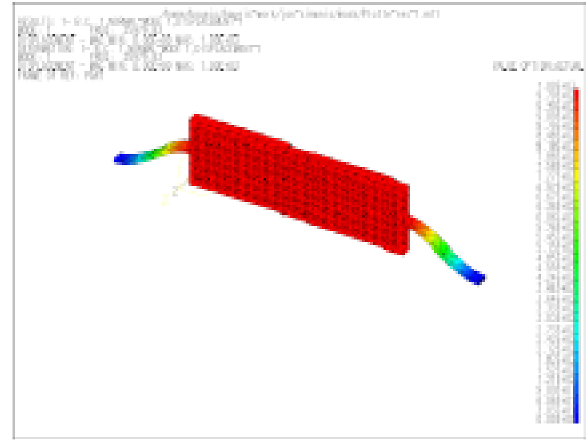

Figure 5 First bending mode at 25.9 kHz (Modal analysis, FEM-IDEAS)

4. Fabrication

The **fabrication** of the packaged resonant structure is done by micromachining processes (Figure 6). Chip Type CAP and chip Type OPT were realized on one and the same wafer. Type CAP and Type OPT sensing cells consist each of three parts: a resonator with handle part (Figure 7), a housing part and a glass lid. The resonator with handle is a SOI wafer with a 2 micrometer oxide and 80 micrometer p-doped device layer. On the device layer the resonator, the electrodes, the connectors from the electrodes to the housing, the alignment springs for glass fibers (Type OPT) and the vacuum channels are integrated. All structures are etched by Deep Reactive Ion Etching (DRIE), which allowed the critical dimension, the minimum comb spacing, to be 5 µm. That is required for keeping the excitation drive voltage low and for maximizing the capacity change during vibration. The silicon sidewall mirror for optical detection in Type OPT was fabricated with an optimized DRIE process. A low surface roughness was achieved by special balancing of the microloading during DRIE through shielding structures in front of the beam at the intended mirror position.

After completition of the SOI wafer etching the removal of the 2 µm oxide layer by 49% HF released the movable parts. Sticking at the 2 µm gap between the mass and the handle wafer is avoided through a sublimation drying step after wet processing. The handle is structured by DRIE as well. The electrodes for circuit connections and the housing layout are determined in this step. The cover part has 250 nm Spin-on-Glass (SOG) on the side, which will face the resonator after bonding [16]. The HF-etch roughened the silicon surface considerably. SOG levels out this roughness and allows bonding. The HF-etch can be avoided, if the movable structures are underetched prior to the Silicon-Direct-Bonding of the SOI. With such a process the resonator and housing can be bonded with thermal oxide instead of SOG in between. The SOG on the housing part was opened by a RIE-step with a subsequent DRIE step 50 micrometer deep, where spacer and trenches for optical fibers (Type OPT) are formed. The backside of the housing was also DRIE through the wafer, given shape to the housing. The resonator part and the housing part were cleaned in Pirania, activated in an oxygen plasma, aligned, mated and underwent a 2 h 1000°C step. The resulting bond connected the housing and the resonator part. The generation of the vacuum is possible through a vacuum anodic-bonding step of a prestructured glass plate on the silicon housing. To guarantee good vacuum stability a getter can be placed in the vacuum cavity prior to the bonding step. In Type OPT, the optical sensor type, the surface roughness of the sidewall where the light from the optical fiber is reflected on has be sufficient low for a low noise Fabry-Perot Interferometer (FPI). The value of roughness improves if overetching in DRIE is minimized. But the optical fiber requires a wide trench, while the electrode combs trenches are only 5 micrometer wide. To overcome this problem the reso-

nator sidewall which builds the FPI therefore was shielded by a wall which was removed after etching. The improvement of the sidewall roughness in shown in Figure 8. The sidewall roughness can furthermore be reduced by an oxidation followed by oxide removal. The oxidation rate on convex surfaces is faster than on concave surface since the oxidation rate depends on local stress. Local stress is concentrated on convex and concave corners [17]. Finally, the chip is connected to the electronics by wire bonding. The optical fiber is inserted in the fiber groove and glued.

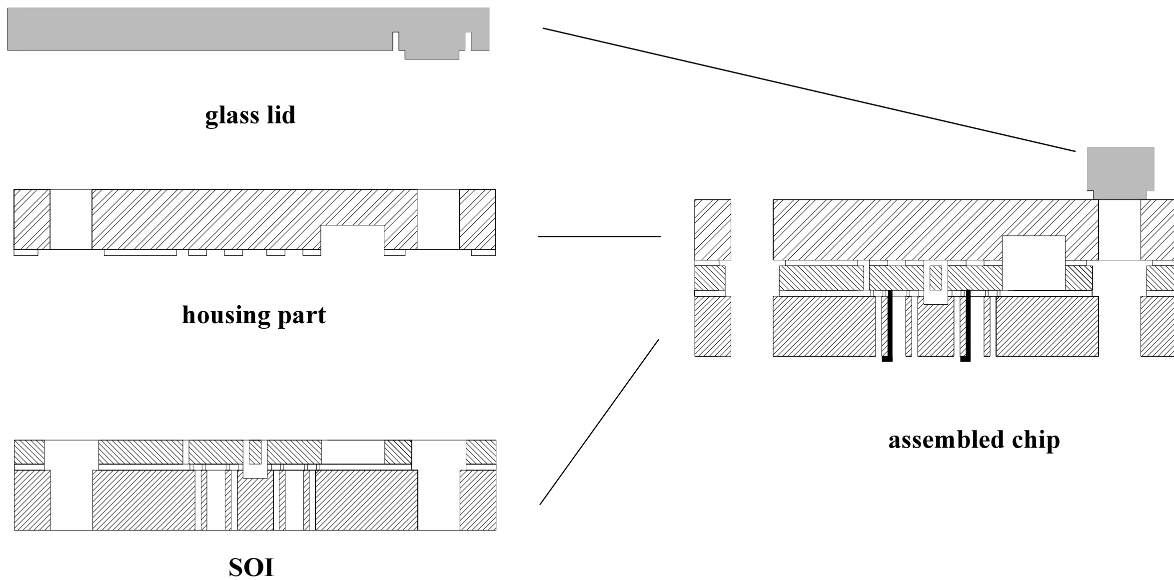

Figure 6 The process steps for the glass lid, the housing part, the resonator on the handle (SOI) and their assembly

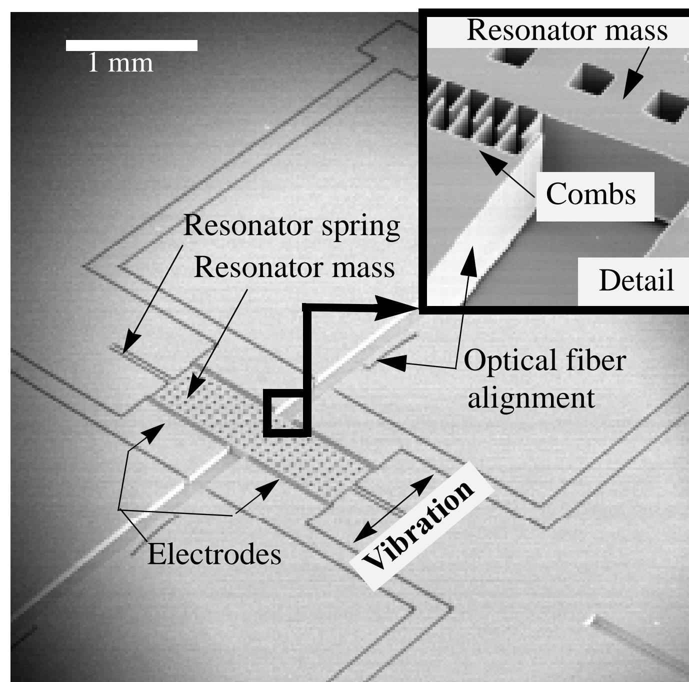

Figure 7 Resonant structure with electrostatic excitation and optical detection

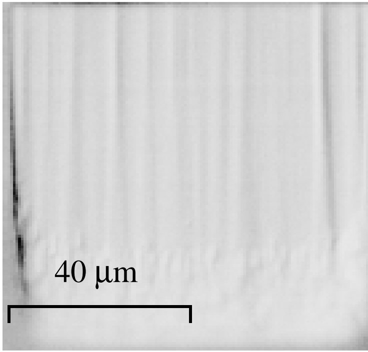

Figure 8 Wall surface at a 150 mm trench

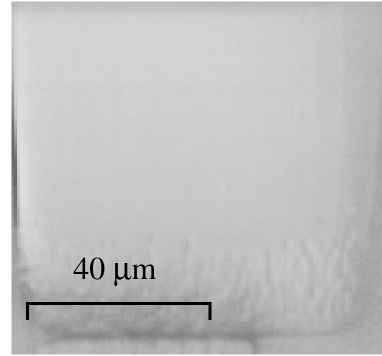

Figure 9 Wall surface in a 20 µm trench

5. Characterization

A **test setup** with a commercial reference force sensor in a vacuum chamber (Figure 13) was used for the investigation of the resonator stability, impact of the fabrication tolerances and the repeatability. The pressure in the chamber is less than 0.1 mbar, so that, according to our theoretical model, the vibration is not further affected by molecular damping. A load sensitivity was as high as 4000 Hz/N (Figure 14). The resonant structure vibrated with an amplitude of 100 nm in resonance and a Q of 30000. A stiffer package increases shunt force and therefore reduces sensitivity with the benefit of increased robustness when mounting the structures in a standard steel housing by Kistler Instrumente AG. Currently we work on an optimization of the shunt force to a minimum necessary for handling and packaging. The difference of the measured resonance frequency from analytical and FEM simulations can be explained by considering the fabrication tolerances in a Rayleigh-Ritz approach. The excitation by an linear electrostatic force generated in a comb drive worked reliable. For the detection we compared capacitive detection and optical detection. Capacitive detection used a switched lock-in amplifier patented at our Institute [10] and introduced for MEMS by Cormann [18]. The signal from the silicon chip is amplified on electronics in SMD technology, brought very close to the chip, connected by wire bonding and mounted together in the housing by Kistler Instrumente AG. The cross talk between the electrodes and the resonator does not affect the measurements, because the excitation is switched off during detection (Figure 10). In contrast to electrical detection the setup for the optical detection is not limited to 100°C. Light from a temperature stabilized laser diode (635 nm) passes a Faraday filter and a fused splitter reaching the resonator. The fiber endface has a 12 nm gold layer, so that refractive index of the fiber end matches the refractive index of the silicon [19]. The back reflected light is coupled by the fused splitter to a photo detector. The results a shown in Figure 11.

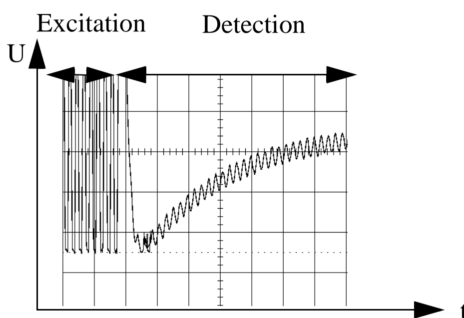

Figure 10 Capacitive detection in closed loop operation with switched lock-in amplifier

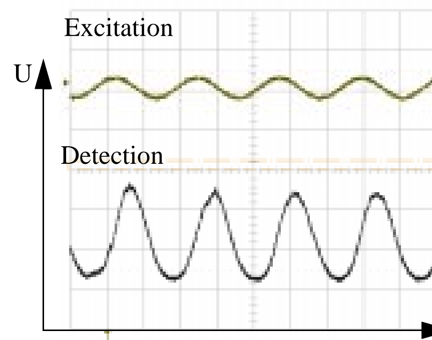

Figure 11 Optical detection of resonance in closed loop

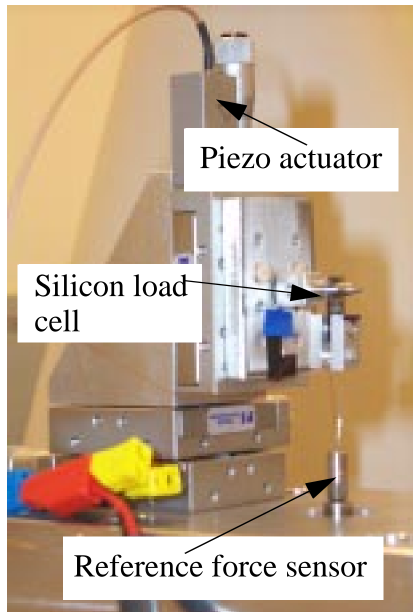

Figure 12 Clamping unit with silicon load cell, piezo for load application and reference force sensor

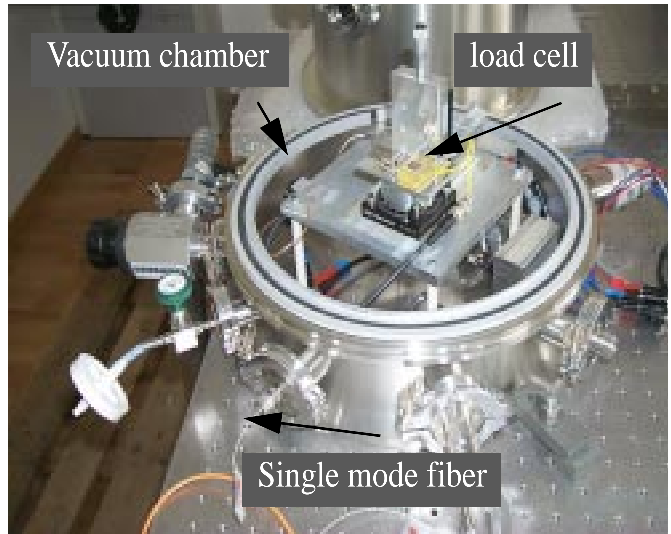

Figure 13 Test setup for testing with optical detection in opened vacuum chamber

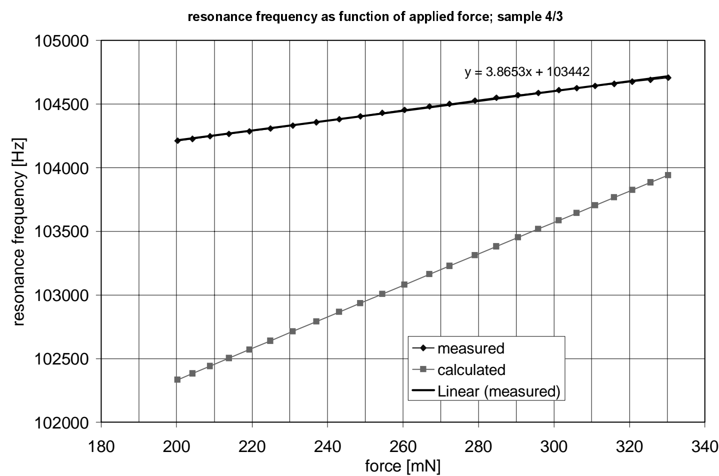

Figure 14 Load-sensitivity: theory and experiment

6. Conclusion

In **summary**, an integrated silicon resonator used as load cell for commercial application and for microstructure characterization was developed. For a temperature up to 100°C a switched lock in amplifier allows off chip charge amplifiers and therefore makes integrated electronics not necessary. Alternatively, optical detection together with the quasi digital output of the

resonator allows safe signal transmission as required by investigations under high temperature and harsh environments. In our experiments we observed on some samples a hysteresis-like behavior. Possible reasons are memory effects in the test setup itself, especially the metal string which connects the silicon cell with the reference force sensor. A stiffer setup will improve that. An other cause we currently look at is the variation of the loading point during stress application [20]. In this case the frame needs to be made insensitive to the contact point between bolt and silicon frame. A possible approach to this is explained in [21].

Acknowledgments

The presented research has been made possible by the Swiss Priority Program in Micro & Nano System Technology. We thank Dr. Gobrecht at PSI (Villigen, CH), Dr. Hunziker at ETH Zürich (Institute of Quantenphysics), Dr. Reiche at MPI (Halle, D), Mr. Clerc at University of Neuchatel (CH) and Dr. Johnston at STS (Newport, UK) for their valuable contributions.

References

[1] Langdon R.M, Resonator sensors - a review, J. Phys. E. Sci. Instrumen.,Vol 18, 1985, 103
[2] Eernisse E.O., Ward R., Wiggins R. B., Survey of Quartz bulk resonator sensors technologies, IEEE Transactions on ultrasonics, ferroelectronics and frequency control, 35, no. 3, May 1988, 323 - 330
[3] Stemme G., Resonant silicon sensors, J. of Micromech. and Microeng., 1, 1991, 113-125
[4] Nguyen CT., Micromachining technologies for miniaturized communication devices, Proceedings of SPIE The International Society for Optical-Engineering. v 3515, 1998, SPIE, Bellingham, WA, USA. 24-38
[5] Blom F.R., Resonant silicon beam force sensor, Ph.D. Thesis, University of Twente, 1989
[6] Tilmans H., Micromechanical sensors using encapsulated built-in resonant strain gauges, Ph.D. Thesis, University of Twente, 1993
[7] Welham Ch., Greenwood J., Bertioli M., A high accuracy resonant pressure sensor by fusion bonding and trench etching, Sensors & Actuators 76, 1999, 298-304
[8] Buser R., Dissertation, University of Neuchatel, 1989
[9] Baltes H., Göpel W., Hesse J., Sensors, Wiley-VCH, Weinheim, 1999, 142-190
[10] Goodbread, J., K. Häusler, M. B. Sayir and J. Dual: Verfahren und Vorrichtung zum Messen derCharakteristik eines Schwingungssystems. Schweiz. Patentanmeldung 657/94-0, 1994
[11] Roszhart T.V., The effect of thermoelastic internal friction on the Q of micromachined silicon resonators, Technical Digest, IEEE - Solid State Sensor and Actuator Workshop 90, Piscataway, USA, 1990, 13-16
[12] Zener C., Internal Friction in Solids, Phys. Rev., 52, 1937, 230-235
[13] Harris C., Crede Ch., Shock and vibration handbook, McGraw-Hill Book Company, New York, 1976, 7.14-7.17
[14] Albert W. C., Vibrating crystal beams accelerometers, Proc. 28.th ISA Int. Instrument. Symp. Las Vegas, NV, USA, May 1982, 33-44
[15] Bouwstra S., Geiijselaers B., On the resonance frequencies of microbridges, Transducers-'91, Int. Conf. Solid State Sens. Actuators, Piscataway, 1991, 538-542
[16] Private communication with Dr. Reiche, Max-Planck-Institut Halle
[17] Microlithography, micromachining, and microfabrication, SPIE optical engineering press, London, 1997, 134-152
[18] Cormann T., Enoksson P., Noren K., Stemme G., Novel burst technology for closed loop detection and excitation of resonant silicon sensors, Transducers 99, Sendai, 1999, CD-ROM
[19] Mayer H., Physik dünner Schichten, Wissenschaftliche Verlagsgesellschaft m.b.H., Stuttgart, 1959
[20] Debnam R.C., Jenkins R.F., The influence of end loading conditions on the performance of strain gauge load cells, 2nd international discussion meeting of the IMEKO sub-committee 'Measurement of force and weight', VDI-Verlag, Dusseldorf, West Germany; 1972, 53-60
[21] Robins G., Load cell shape optimization using genetic algorithms and finite element analysis, State of the art in force an mass measurement, Proceedings of the 14 th IMEKO TC3 Conference, Warsaw, Poland, 1995, 167-172

Appendix I

The space solution of is:

$$y_n = C_1 \cdot Sinh\left[\frac{k_n}{l} \cdot x\right] + C_2 \cdot Cosh\left[\frac{k_n}{l} \cdot x\right] + C_3 \cdot Sin\left[\frac{k_n}{l} \cdot x\right] + C_4 \cdot Cos\left[\frac{k_n}{l} \cdot x\right]$$

where k_n = wave number of mode n, C_1, C_2, C_3, C_4 = constants.
Flexural potential energy E_{pm}, Axial Force potential energy E_{pf}, Shear potential energy E_{pv}, Linear kinetic energy E_{kl} ::

$$E_{pm} = \frac{E \cdot I}{2} \cdot \int_0^{\frac{l}{2}} (y'')^2 dx \,,\; E_{pf} = \frac{F}{2} \cdot \int_0^{\frac{l}{2}} (y')^2 dx \,,$$

$$E_{pv} = \frac{3(E \cdot I)^2}{4 \cdot G \cdot A} \cdot \int_0^{\frac{l}{2}} (y''')^2 dx \,,\; E_{kl} = \frac{\omega^2 \cdot A \cdot \rho}{2} \cdot \int_0^{\frac{l}{2}} y^2 dx + \omega^2 \cdot \frac{m}{4} \cdot y^2(0)$$

with ρ = density and rotational energy E_{kr} :

$$E_{kr} = \frac{\rho \cdot I \cdot \omega^2}{2} \cdot \int_0^{\frac{l}{2}} (y')^2 dx + \omega^2 \cdot \frac{\theta}{4} \cdot y'^2(0)$$

where θ = moment of rotational inertia.
For the total energy in the system we receive:

$$E_{pf} + E_{pm} + E_{pv} = E_{kr} + E_{kl}$$

In [14] was shown that only for high ratios of beam thickness/length and for high modes the shear and rotational energy needs to be considered. If therefore shear potential energy and rotational energy are neglected in the first approximation for the first bending mode and the resonant frequency is determined by:

$$\omega = \omega_o \left[1 + \frac{F \cdot \int_0^{\frac{l}{2}} (y')^2 dx}{\omega_o^2 \left(A \cdot \rho \int_0^{\frac{l}{2}} y^2 dx + \frac{m}{2} \cdot y^2(0) \right)} \right]^{\frac{1}{2}} ,\; \omega_o^2 = \frac{E \cdot I \int_0^{\frac{l}{2}} (y'')^2 dx}{A \cdot \rho \int_0^{\frac{l}{2}} y^2 dx + \frac{m}{2} \cdot y^2(0)}$$

The integral expressions are:

$$y^2(0) = \left(C_4 \cdot \left(\frac{C_2}{C_4} Cosh[0] + Cos[0] \right) \right)^2 = C_y \cdot C_4^2 \text{ and } C_y = 1.28$$

$$\int_0^{\frac{l}{2}} (y')^2 dx = 3.11 \frac{C_4^2}{l} \,,\; \int_0^{\frac{l}{2}} (y'')^2 dx = 127 \frac{C_4^2}{l^3} \,,\; \int_0^{\frac{l}{2}} y^2 dx = 0.254 \cdot C_4^2 \cdot l$$

The resonance frequency for a loaded beam - mass structure becomes:

$$\omega = \omega_o\left[1 + \frac{0.025 \cdot l^2 \cdot F}{E \cdot I}\right]^{\frac{1}{2}}, \ \omega_o = \sqrt{127 \cdot \frac{E \cdot I}{l^3} \cdot \frac{1}{m'_A \cdot 0.254 \cdot l + 0.5 \cdot m \cdot C_y}}$$

The sensitivity ratio r_S between a single beam and a mass suspended by beams is:

$$r_S = \left|\frac{\int_0^{\frac{l}{2}} (y')^2 dx}{E \cdot I \int_0^{\frac{l}{2}} (y'')^2 dx}\right|_{beamA} \left(\left|\frac{\int_0^{\frac{l}{2}} (y')^2 dx}{E \cdot I \int_0^{\frac{l}{2}} (y'')^2 dx}\right|_{beamB}\right)^{-1} \quad \text{or simplified } r_S = \frac{\left|\frac{1}{E \cdot I} \cdot l^2\right|_{beamA}}{\left|\frac{1}{E \cdot I} \cdot l^2\right|_{beamB}}$$

The resonance freqency for a single beam is:

$$\omega_{oB} = \left(\frac{\lambda}{l_B}\right)^2 \sqrt{E \cdot I \cdot \frac{1}{m'_B}}$$

where λ = mode number and l_B .= length of beam “B”. Assuming for both, the beam with the mass in its center and the simple clamped beam same material and momentum of bending inertia and that the mesa mass is much greater than the beam mass we receive for the simple beam lenght:

$$l_B = 0.063 \cdot \lambda \cdot \left(\frac{m'_A}{m'_B}\right)^{\frac{1}{4}} \cdot l_A^{\frac{3}{4}} \cdot \left(127 \cdot l_A + 250 \cdot C_y \cdot \frac{m}{m'_A}\right)^{\frac{1}{4}}$$

Finally, the sensitivity ratio becomes for the first bending mode:

$$r_S = \sqrt{\frac{m'_B}{m'_A}} \cdot \frac{1}{\sqrt{1 + \frac{250}{127} \cdot \frac{m}{m'_A} \cdot \frac{1}{l_A}}} .$$